PAPER

The difference of roles of alkaline-earth metal oxides on silica-supported nickel catalysts for CO$_2$ methanation

Meng Guo[ab] and Gongxuan Lu[*a]

The roles of alkaline-earth metal oxides on CO$_2$ methanation over modified Ni/SiO$_2$ catalysts were investigated. Ni/MO/SiO$_2$ catalysts with variable elements (M = Mg, Ca, Sr and Ba) were prepared by the sequential impregnation method. The results indicated that the presence of SrO promoted the catalytic activity and enhanced the catalyst stability. In addition, BaO addition enhanced the reaction activity, but the Ni/BaO/SiO$_2$ catalyst deactivated significantly after 50 h of time-on-stream due to the sintering of metallic Ni. Moreover, CaO addition affected negligibly the performance of the Ni/CaO/SiO$_2$ catalyst, and MgO addition inhibited significantly the methanation performance because of the low reducibility of Ni species.

1 Introduction

Nowadays, the ~395 ppm level of CO$_2$ in the atmosphere has caused a lot of severe environmental problems. To mitigate them, capture and conversion of CO$_2$ have been investigated extensively. Processes related to CO$_2$ chemical utilization, such as providing various commodity chemicals and renewable fuels, have been proposed.[1–9] It is well known that methane as a renewable fuel can be produced from the Sabatier reaction, *i.e.*, hydrogenation of CO$_2$ to methane. If hydrogen in this reaction is provided by solar energy, for example, *via* water photolysis, the sustainable cycle can be achieved.

The Ru, Rh and Pd catalysts supported on Al$_2$O$_3$, TiO$_2$ and MgO *etc.*, have exhibited excellent catalytic properties in CO$_2$ methanation,[5,10–12] among which Ru is the most active component at low temperature.[13] Some supported or non-supported transition metal catalysts have acceptable performance, such as Ni,[8,9,14–19] Co[20–23] and Fe.[20,24] Moreover, the promotion effect of second transition metal addition to the Ni-based catalysts has also been reported.[25,26] If a proper amount of Mo is added to the Ni-based catalysts, both the catalytic activity and selectivity of CH$_4$ can be enhanced. It can be attributed to the formation of MoOx species, which not only promotes Ni metal particle dispersion, but also assists the partial electron transfer to Ni sites.[25]

Depending on the catalytic system considered, alkaline-earth metal oxides act as structural promoters by increasing the dispersion of the active phase and stabilizing the dispersed

metallic phase against sintering.[19,27–29] In addition, these additives also act as chemical promoters by influencing the acid–base properties of support[30–32] or the electron density of dispersed metal crystallites.[33,34] Park *et al.* have revealed that MgO can initiate the reaction by binding CO$_2$ molecules *via* forming magnesium carbonate species on the catalyst surface. The supply of hydrogen atoms is essential for hydrogenation of magnesium carbonate to CH$_4$.[30,31]

In this work, the effect of alkaline-earth metal oxides (MgO, CaO, SrO and BaO) with the same controlled contents of Ni/SiO$_2$ catalyst for CO$_2$ methanation are reported. The results indicate that the effect of alkaline-earth metal oxides was quite different. Therefore, the results are discussed by considering the roles of alkaline-earth metal-induced alterations of Ni/SiO$_2$ catalysts on the physicochemical characteristics. The catalytic activity and catalyst stability are also discussed to develop the catalysts with enhanced activity and stability.

2 Experimental

2.1 Catalyst preparation

Using Ni(NO$_3$)$_2$·6H$_2$O as a metal precursor, 10 wt% Ni/SiO$_2$ (denoted as Ni/Si) catalyst was prepared by wet impregnation followed by spontaneous dispersion upon calcination. Prior to impregnation, the support SiO$_2$ (20–45 mesh) was calcined at 500 °C for 6 h. After calcination, its specific area was 438 m^2 g^{-1}. The aqueous solution containing an appropriate amount of Ni(NO$_3$)$_2$ was mixed with the calculated amount of support. After the impregnation for 24 h, the precursor mixture was dried further at 110 °C for another 24 h, and then calcined at 500 °C for 6 h in an oven.

10 wt% Ni/4 wt% MO/SiO$_2$ (M = Mg, Ca, Sr and Ba) catalysts were denoted as se-Ni/M/Si catalysts and prepared by the

[a]*State Key Laboratory for Oxo Synthesis and Selective Oxidation, Lanzhou Institute of Chemical Physics, Chinese Academy of Sciences, Lanzhou 730000, P.R. China. E-mail: gxlu@lzb.ac.cn; Tel: +86 931 4968178*

[b]*University of Chinese Academy of Sciences, Beijing 100049, P.R. China*

sequential impregnation method, in which impregnation of an aqueous solution containing appropriate amount of $Mg(NO_3)_2$, $Ca(NO_3)_2$, $Sr(NO_3)_2$, or $Ba(NO_3)_2$ was followed by heat treatment and then by impregnation of nickel nitrate aqueous solution.[35] The two drying and calcination procedures were the same as for the Ni/Si catalyst.

2.2 Catalytic activity measurements

The catalytic performance was carried out in a fixed bed continuous flow quartz reactor (i.d. 8 mm) using a mixture of H_2 and CO_2 at molar ratio of 4 balanced with N_2 (30 ml min^{-1}), which is depicted in Fig. 1. Typically, 0.2 g of catalyst was used in each turn at GHSV of 15 000 ml h^{-1} g^{-1}. Prior to a test, the fresh catalyst was reduced *in situ* for 3 h under a 50 vol% H_2–N_2 mixture (60 ml min^{-1}) and then cooled down to room temperature under the same conditions. The effluent mixed gases were cooled in an ice-water trap to remove the gaseous water generated. The effluent gases were collected after half an hour of steady-state operation, and the their separation and quantification were attained on two on-line chromatographs equipped with thermal-conductivity detectors (TCD). Nitrogen was used as a carrier gas and internal standard for gas analysis. Experimental error was typically within ±4%. The conversion of CO_2 and the selectivity to the products were calculated based on the balance of carbon, which was estimated within 100% ± 1%. CO_2 conversion (X_{CO_2}), CH_4 selectivity (S_{CH_4}) and CO selectivity (S_{CO}) are described as follows:

$$X_{CO_2} = (F_{CO_2in} - F_{CO_2out})/F_{CO_2in} \tag{1}$$

$$S_{CH_4} = F_{CH_4out}/(F_{CH_4out} + F_{COout}) \tag{2}$$

$$S_{CO} = F_{COout}/(F_{CH_4out} + F_{COout}) \tag{3}$$

2.3 Catalyst characterization

Hydrogen-temperature programmed reduction (H_2-TPR) measurements were carried out by heating a sample (50 mg) at 10 °C min^{-1} in a flow of 5 vol% H_2/Ar gas mixture (40 ml min^{-1}). The amount of consumed hydrogen was measured by TCD.

X-ray diffraction (XRD) was performed on the selected samples using Cu Kα radiation (Philips X'pert MPD instrument) at a scattering rate of 4° min^{-1} at 40 mA and 50 kV.

The chemical states of the atoms on the catalyst surface were investigated by X-ray photoelectron spectroscopy (XPS) on a VG ESCALAB 210 Electron Spectrometer (Mg Kα radiation; $hv = 1253.6$ eV). XPS data were calibrated using the binding energy of the Si 2p (103.4 eV) as a standard.

Transmission electron microscopy (TEM) images were obtained using the FEI F20 (Netherlands) high-resolution transmission electron microscopy operating at an accelerating voltage of 200 kV. The sample for TEM analyses was treated ultrasonically in ethanol and then transferred as a suspension to a carbon-coated copper grid.

3 Results and discussion

3.1 H_2-TPR analysis

H_2-TPR measurements were conducted to understand the reduction behavior of metal oxide-based supported catalysts, which could further provide information about the interactions between metal oxides and their supports. Profiles of H_2-TPR for the as-synthesized bare and modified Ni/SiO$_2$ materials are
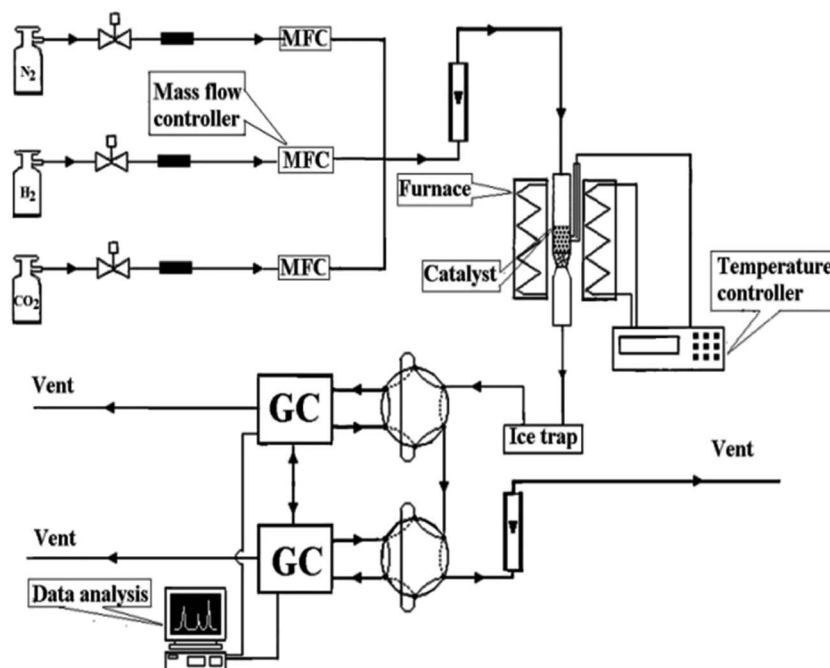

Fig. 1 Schematic diagram of the experimental system.

presented in Fig. 2 and the quantitative data of Ni species are given in Table 1, where significant effects of alkaline-earth metal oxides on the reduction behavior of the Ni species were observed. TPR profile of Ni/Si catalyst was composed of a sharp peak and a shoulder peak. This sharp peak consisted of two maxima at 395 (α peak, 27%) and 424 °C (β peak, 43%). The two peaks were attributed to the reduction of some inhomogeneous NiO phases that interacted weakly with the silica.[36,37] The shoulder peak at 484 °C (γ peak, 30%) could be attributed to the stronger interactions between the bulk NiO phase and the support.[38,39] The initial reduction temperature increased from 350 °C of Ni/Si catalyst to 440 °C of se-Ni/Mg/Si catalyst, 385 °C of se-Ni/Ca/Si catalyst, and 365 °C of se-Ni/Sr/Si catalyst. In addition, for all the modified Ni/SiO₂ catalysts, the reduction peaks of alkaline-earth metal-modified Ni/SiO₂ materials migrated gradually toward higher temperatures. For se-Ni/Mg/Si sample, the peaks are constituted by two maxima at 456 (γ peak, 1%) and 634 °C (ε peak, 99%). For the se-Ni/Ca/Si material, two broad reduction peaks were observed, which consists of different peaks at 435 (β peak, 17%), 472 (γ peak, 34%), 588 (δ peak, 31%) and 640 °C (ε peak, 9%). In addition, the H₂-uptake ratios of Ni/Si, se-Ni/Mg/Si and se-Ni/Ca/Si catalysts were 1 : 0.3 : 0.8. For se-Ni/Sr/Si and se-Ni/Ba/Si catalysts, H₂-TPR profiles were similar and the area of the high temperature peaks increased evidently, which indicated that the amount of the more stable Ni species increased. In addition, the H₂-uptake ratios of Ni/Si, se-Ni/Sr/Si and se-Ni/Ba/Si catalysts were 1 : 1.1 : 1.3.
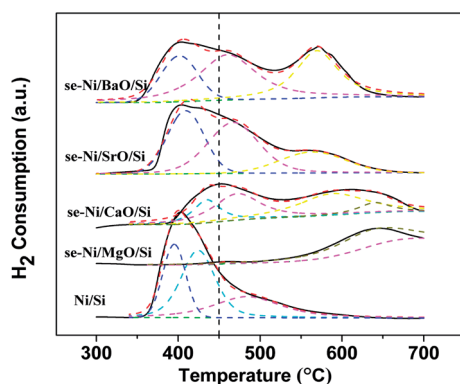

Fig. 2 H₂-TPR profiles of fresh catalysts.

Table 1 H₂-TPR quantitative data of fresh catalysts

Samples	T_m (°C)					Fraction of total area (%)				
	α	β	γ	δ	ε	α	β	γ	δ	ε
Ni/Si	395	424	484	—	—	27	43	30	—	—
se-Ni/Mg/Si	—	—	456	—	634	—	—	1	—	99
se-Ni/Ca/Si	—	435	472	588	640	—	17	34	31	9
se-Ni/Sr/Si	409	—	467	564	—	35	—	44	24	—
se-Ni/Ba/Si	401	—	460	569	—	21	—	45	30	—

3.2 XRD analysis

XRD patterns of bare and modified Ni/SiO₂ catalysts pretreated in a 50 vol.% H₂–N₂ mixture (60 ml min⁻¹) at 450 °C for 3 h are presented in Fig. 3. The typical broad diffraction peaks of SiO₂ support could be observed. For the Ni/Si catalyst, the diffraction peaks located at $2\theta = 44.5°$, 51.8° and 76.4° (JCPDC Card no. 87-0712), indicate the existence of the characteristics of Ni metal phase.[17,40] The NiO peaks were located at $2\theta = 37.2°$, 43.3° and 62.8° (JCPDC Card no. 89-5881), which suggested that some NiO species exist in the bulk phase of the catalysts.[19,41] In addition, the relative intensity of diffraction peaks of metallic Ni and NiO phases was 5.76. The diffraction peaks of Ni metal were very sharp, which indicated that Ni crystal phases were comparatively well crystallized. By comparison to Mg-modified Ni/SiO₂ catalyst, it was found that the XRD peaks could be attributed to NiO and MgO mixed phases (near 37.2°, 43.3° and 62.8°, JCPDC Card no. 03-0988) and small amounts of Ni phase (near 44.5°, 51.8° and 76.4°). For the se-Ni/Ca/Si, se-Ni/Sr/Si and se-Ni/Ba/Si catalysts, the relative intensities of the diffraction peaks of metallic Ni and NiO phases were 0.97, 3.42 and 4.19, respectively, which suggested that Ni species over alkaline-earth metal-modified Ni/SiO₂ catalysts were more difficult to be reduced than those over Ni/Si catalyst under some given conditions. Moreover, there was Ba₄Si₆O₁₆ diffraction peak observed in the se-Ni/Ba/Si catalyst. In addition, the metallic Ni particle sizes on the Ni/Si, se-Ni/Mg/Si, se-Ni/Ca/Si, se-Ni/Sr/Si and se-Ni/Ba/Si catalysts estimated from XRD of the peaks at $2\theta = 44.5°$ calculated by the Scherrer formula were 50.9, 19.6, 35.8, 36.9 and 45.2 nm. It demonstrated that alkaline-earth metal oxides enhanced the dispersion of nickel species.

3.3 XPS analysis

The chemical element states of surface species on the materials could be investigated commonly by XPS experiment. Therefore, XPS measurement was performed. The results related with binding energies of Ni 2p₃/₂ and the derived atomic composition in the different samples were analyzed and are summarized in Fig. 4 and Table 2, respectively. It was found that the binding energies of the surface Ni 2p₃/₂ species were affected
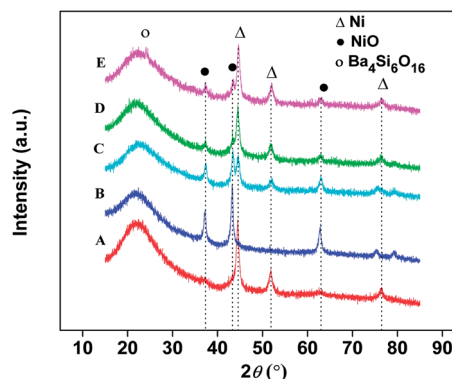

Fig. 3 XRD results of catalysts reduced at 450 °C: A, Ni/Si; B, se-Ni/Mg/Si; C, se-Ni/Ca/Si; D, se-Ni/Sr/Si; E, se-Ni/Ba/Si.
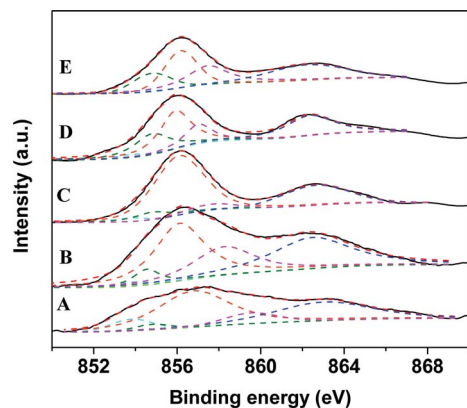
Fig. 4 XPS spectra of Ni 2p$_{3/2}$ over fresh catalysts: A, Ni/Si; B, se-Ni/Mg/Si; C, se-Ni/Ca/Si; D, se-Ni/Sr/Si; E, se-Ni/Ba/Si.

significantly by modified alkaline-earth metal oxides. Moreover, the relative contents of the nickel species changed significantly, as shown in Table 2. For the modified catalysts, the peaks of binding energies of Ni 2p$_{3/2}$ were mainly distributed around 853.8, 854.8 and 856.1 eV, which could be assigned to different types of NiO species.[42] The two higher binding energies of Ni 2p$_{3/2}$ (around 858 and 863 eV) could be assigned to the shake-up satellite peaks of NiO species. Over the Ni/Si catalyst surface, the 49.3% of NiO(γ) species was dominant. For se-Ni/Mg/Si and se-Ni/Ca/Si catalysts, the NiO(γ) species contents could increase to 49.6% and 62.5%, respectively. However, for se-Ni/Sr/Si and se-Ni/Ba/Si catalysts, the NiO(γ) species contents could decrease to 34.0% and 29.9%, respectively. The XPS results of the samples in Table 2 demonstrated that Ni species increased on the modified catalyst surface with the modification of alkaline-earth metal oxides, as observed by the higher surface Ni/Si ratio. Furthermore, the change of surface Ni/M (M = Mg, Ca, Sr or Ba) ratio also indicated that the modified alkaline-earth metal oxides could be dispersed effectively on SiO$_2$ supports.

3.4 Study of GHSV over Ni/Si catalyst

Prior to all the catalytic experiments, a blank test was carried out firstly and it did not show any catalytic activity, even at temperatures as high as 500 °C. Then, in order to optimize the catalyst amount loaded into the reactor, GHSV was ranged from 7500 to 60 000 ml h^{-1} g^{-1}. The catalytic performances of the Ni/

Si catalyst under typical reaction conditions (H$_2$/CO$_2$ molar ratio = 4; P = 1 atm) were tested at these GHSV and temperatures ranging from 200 to 500 °C. The results of CO$_2$ conversions and product distributions are presented in Fig. 5. As shown in Fig. 5a, when the reaction temperature was below 300 °C, the conversions were less than 50.6%. When the reaction temperature increased to 400 °C, CO$_2$ conversions ended up at 49.1%, 61.3%, 70.9%, 73.2%, 77.4% and 81.3% over CHSV of 60 000, 30 000, 20 000, 15 000, 10 000 and 7500 ml h^{-1} g^{-1}, respectively. Moreover, at 350 and 400 °C and GHSV of 10 000 ml h^{-1} g^{-1}, the similar CO$_2$ conversions were 74.9% and 77.4%, respectively, which indicated that working at 350 °C was optimal considering CH$_4$ selectivities and the high temperature sintering of the metallic Ni.[43]

3.5 Catalytic performances over alkaline-earth metal-modified Ni/SiO$_2$ catalysts

The catalytic performances of the bare and modified Ni/SiO$_2$ catalysts were investigated at temperatures ranging from 300 to 450 °C under the given reaction conditions (GHSV = 15 000 ml h^{-1} g^{-1}, H$_2$/CO$_2$ molar ratio = 4 and P = 1 atm). Reaction temperature influenced significantly the catalytic behaviors.[15–24] As shown in Table 3, CO$_2$ conversions depended largely on the reaction temperatures. At 350 °C, carbon dioxide conversions were low and the reaction produced mostly CH$_4$ with small amounts of by-product CO.[43,44] With temperature increased to 450 °C, the catalytic activities were improved. The addition of MgO to Ni/SiO$_2$ showed remarkable inhibition effects on the catalytic activity, and increasing temperature to 350 °C or higher showed no promotion effects on the catalytic activity for se-Ni/Ca/Si catalyst. In comparison, SrO and BaO improved both the catalytic activity and CH$_4$ selectivity. Compared with Ni/Si catalyst, less metallic Ni species were presented on the SrO and BaO modified catalysts, which indicated that the SrO and BaO should be responsible for the superior catalytic performances of se-Ni/Sr/Si and se-Ni/Ba/Si catalysts. However, MgO addition demonstrated remarkable negative effects on the catalytic activity due to the very low reducibility of the metallic Ni species.[19]

3.6 Stability test

The research of catalyst stability tests had become an important issue in CO$_2$ methanation to realize its industrialized

Table 2 XPS results of fresh catalysts

| Samples | B.E. (Ni 2p$_{3/2}$) (eV) | | | | | Fraction of total area (%) | | | | | Ni/Si^a | M/Si^a |
	α	β	γ	δ	ε	α	β	γ	δ	ε		
Ni/Si	853.8	854.8	856.8	859.5	863.0	7.1	2.8	49.3	9.4	31.3	0.015	0
se-Ni/Mg/Si	853.8	854.8	856.1	859.6	862.8	6.7	2.9	49.6	8.2	30.5	0.034	0.120
se-Ni/Ca/Si	853.8	854.8	856.1	857.7	862.7	1.7	7.1	62.5	4.9	23.7	0.044	0.144
se-Ni/Sr/Si	853.8	854.8	855.9	857.0	862.4	2.9	20.7	34.0	15.0	27.4	0.056	0.088
se-Ni/Ba/Si	853.8	854.8	856.2	857.5	862.3	1.6	15.9	29.9	24.7	27.9	0.047	0.071

^{a} Calculated by Ni (or M = Mg, Ca, Sr or Ba) atom%/Si atom% from XPS spectra.

application. As for CO_2 methanation, its fatal drawback was that the catalysts were mainly subjected to the deactivation mechanisms caused by the sintering and/or oxidation of the metallic phase, which could lead to the decrease of the active metal sites on the catalyst surface and ultimately influence the catalyst stability. Therefore, multiple catalyst performances at 50 h were monitored by means of CO_2 conversions and of CH_4 selectivities. The evaluation of the long-term catalyst stabilities was performed under specific reaction conditions: 350 °C, GHSV = 15 000 ml h^{-1} g^{-1}, H_2/CO_2 molar ratio = 4 and P = 1 atm. The Ni/Si, se-Ni/Sr/Si and se-Ni/Ba/Si catalysts were selected as the typical catalysts. The results of catalyst stability and deactivation are shown in Fig. 6. As shown in Fig. 6, at the beginning, Ni/Si, se-Ni/Sr/Si and se-Ni/Ba/Si catalysts exhibited 64.7%, 70.5%
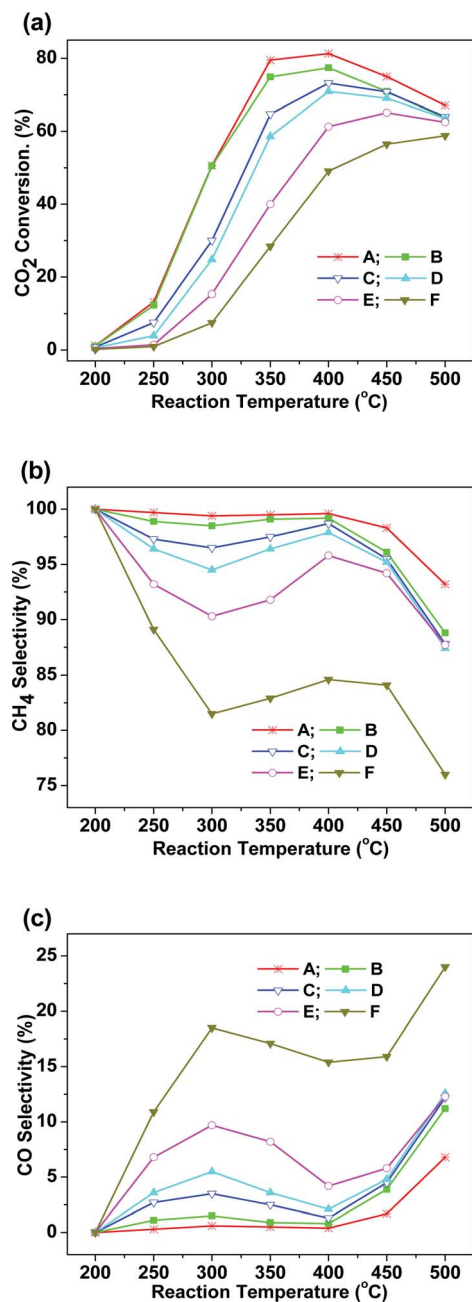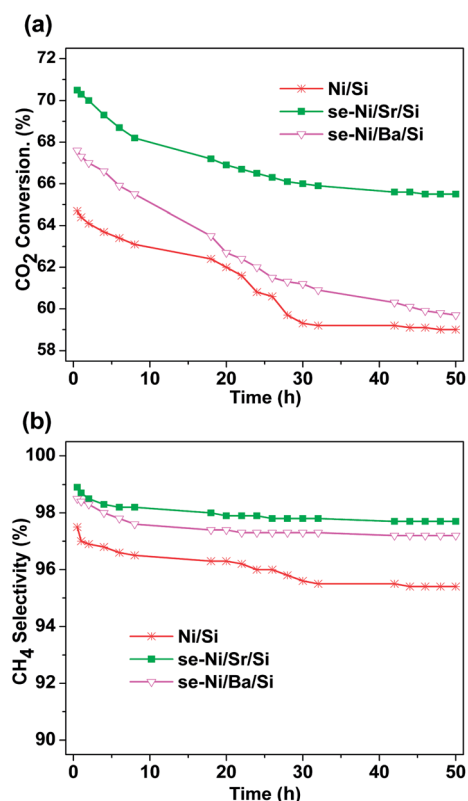

Fig. 5 Catalytic performance of Ni/Si catalyst at various temperatures and different GHSV: A, 7500; B, 10 000; C, 15 000; D, 20 000; E, 30 000; F, 60 000 ml h^{-1} g^{-1}. Reaction conditions: H_2/CO_2 molar ratio = 4; P = 1 atm.

Fig. 6 Long-term stability tests at 350 °C. Reaction conditions: GHSV = 15 000 ml h^{-1} g^{-1}; H_2/CO_2 molar ratio = 4; P = 1 atm.

Table 3 Catalytic performance of alkaline-earth metal-modified Ni catalysts at different temperatures. Reaction conditions: GHSV = 15 000 ml h^{-1} g^{-1}; H_2/CO_2 molar ratio = 4; P = 1 atm

	300 °C			350 °C			400 °C			450 °C		
Samples	X_{CO_2}	S_{CH_4}	S_{CO}	X_{CO_2}	S_{CH_4}	S_{CO}	X_{CO_2}	S_{CH_4}	S_{CO}	X_{CO_2}	S_{CH_4}	S_{CO}
Ni/Si	27.0	94.5	5.5	64.7	97.5	2.5	73.2	98.7	1.3	70.8	95.5	4.5
se-Ni/Mg/Si	8.7	87.1	12.9	34.9	85.3	14.7	61.9	92.1	7.9	62.0	90.1	9.9
se-Ni/Ca/Si	37.2	97.2	2.8	64.9	98.6	1.4	73.3	98.9	1.1	70.6	95.4	4.6
se-Ni/Sr/Si	39.4	97.6	2.4	70.5	98.9	1.1	76.3	99.0	1.0	72.4	97.5	2.5
se-Ni/Ba/Si	38.3	97.4	2.6	67.6	98.5	1.5	74.9	98.9	1.1	72.2	97.3	2.7

and 67.6% conversions to CO_2 and 97.5%, 98.9% and 98.5% selectivities to CH_4 at 0.5 h, respectively. In addition, compared to Ni/Si and se-Ni/Ba/Si catalysts, se-Ni/Sr/Si catalyst exhibited higher CO_2 conversions, higher CH_4 selectivities and more stable catalytic behavior in the entire 50 h time on stream.[7,19] At 50 h, CO_2 conversions of Ni/Si, se-Ni/Sr/Si and se-Ni/Ba/Si catalysts were 59.0%, 65.5% and 59.7% and CH_4 selectivities of these catalysts were 95.4%, 97.7% and 97.2%, respectively. This indicated that se-Ni/Sr/Si catalyst might be a better candidate as compared to Ni/Si and se-Ni/Ba/Si catalysts. Therefore, SrO addition is a more effective method to promote higher catalytic performances.

The XRD patterns of the selected catalysts after 50 h of reaction are comparatively plotted in Fig. 7. Compared to the reduced Ni/Si and se-Ni/Ba/Si catalysts, the average particle sizes of Ni phases in the used catalyst increased by about 10.7 and 8.1 nm, and the intensities of Ni and NiO phases decreased to 4.45 and 3.55, respectively. This indicated that not only the metallic Ni phase sintered, but the metallic Ni species on the catalyst surface could oxidize to NiO in the reaction process, which lowers the catalytic stability. The metallic Ni particle size of the used se-Ni/Sr/Si catalyst estimated from XRD of the peaks at $2\theta = 44.5°$ was 41.9 nm, and the intensities of Ni and NiO phases were 3.88. This demonstrated that in the reaction process, modified SrO could inhibit the sintering of metallic Ni on the catalyst surface to some extent, which was in agreements with the results of the stability test. Moreover, the diffraction peaks located at $2\theta = 25.2°$, $36.3°$ and $50.0°$ (JCPDC Card no. 01-0556) indicated the existence of the characteristics of a $SrCO_3$ phase, which might lead to the reduction of NiO species. Moreover, for CO_2 methanation, catalyst surface restructuring might be influenced by the feed gases,[45] products,[46,47] new species,[48] etc. In addition, the combination of metal cultures and particles on the Sr-based oxides were frequently reported.[49–51] With the help of oxygen affinity, Ni atoms could react with substrate O atoms, resulting in the reduction of the high interfacial strain.[52,53]

To understand further the roles of the SrO addition in the used se-Ni/Sr/Si catalyst, TEM analysis of the 50 h endurance-tested catalyst at 350 °C was carried out. As shown in Fig. 8a and
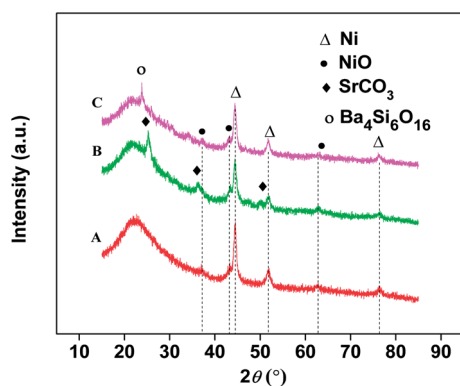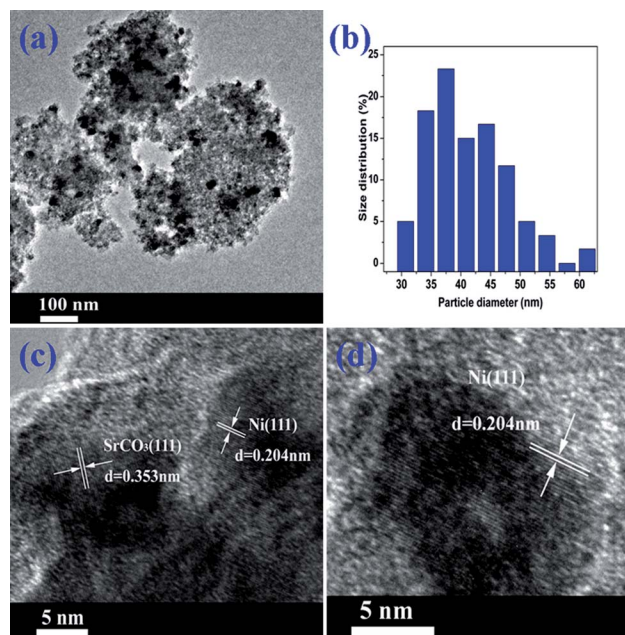
Fig. 8 (a) Low magnification, and (c and d) high magnification TEM images of the 50 h endurance-tested se-Ni/Sr/Si catalyst at 350 °C; (b) size distribution obtained from (a).

b, the average size of Ni particles in the used se-Ni/Sr/Si catalyst was 37.5 nm based on 100 particles, which was very similar to the value estimated by XRD. This indicated further that the presence of SrO could inhibit the metallic Ni sintering. The d-spacings of Ni(111) and $SrCO_3$(111) are also given in Fig. 8c and d. These results may also demonstrate that the reason for the NiO species reduction in the reaction process was the formation of $SrCO_3$ phase.

4   Conclusion

Carbon dioxide methanation reaction was studied over a series of Ni/SiO$_2$ catalysts modified with alkaline-earth metal oxides (MgO, CaO, SrO and BaO). MgO addition inhibited the catalytic property of the se-Ni/MgO/Si catalyst significantly due to the low reducibility of the nickel species. The presence of CaO addition affected the reaction performance negligibly. However, SrO modification promoted the catalytic activity, and enhanced the catalyst stability because it inhibits metallic Ni sintering. Moreover, BaO addition enhanced the catalytic activity, but se-Ni/Ba/Si catalyst deactivated significantly because of the sintering of metallic Ni phase.

Acknowledgements

Fig. 7 XRD patterns of used Ni-based catalysts at 350 °C after 50 h: A, Ni/Si; B, se-Ni/Sr/Si; C, se-Ni/Ba/Si.

References

1 J. Gao, Y. Wang, Y. Ping, D. Hu, G. Xu, F. Gu and F. Su, *RSC Adv.*, 2012, **2**, 2358–2368.

2 B. Lu and K. Kawamoto, *RSC Adv.*, 2012, **2**, 6800–6805.

3 O. G. Griffiths, R. E. Owen, J. P. O'Byrne, D. Mattia, M. D. Jones and M. C. McManus, *RSC Adv.*, 2013, **3**, 12244–12254.

4 F. Ding, A. Zhang, M. Liu, X. Guo and C. Song, *RSC Adv.*, 2014, **4**, 8930–8938.

5 F. Wang, S. Zhang, C. Li, J. Liu, S. He, Y. Zhao, H. Yan, M. Wei, D. G. Evans and X. Duan, *RSC Adv.*, 2014, **4**, 10834–10840.

6 Z. Liu, Y. Wang, J. Li and R. Zhang, *RSC Adv.*, 2014, **4**, 13280–13292.

7 Z. Shen, M. Gu, M. Zhang, W. Sang, X. Zhou, Y. Zhang and F. Jin, *RSC Adv.*, 2014, **4**, 15256–15263.

8 W. Zhen, B. Li, G. Lu and J. Ma, *RSC Adv.*, 2014, **4**, 16472–16479.

9 Y. Li, G. Lu and J. Ma, *RSC Adv.*, 2014, **4**, 17420–17428.

10 W. Wang, S. Wang, X. Ma and J. Gong, *Chem. Soc. Rev.*, 2011, **40**, 3703–3727.

11 S. Sharma, Z. Hu, P. Zhang, E. W. McFarland and H. Metiu, *J. Catal.*, 2011, **278**, 297–309.

12 A. Karelovic and P. Ruiz, *J. Catal.*, 2013, **301**, 141–153.

13 D. J. Darensbourg, C. Ovalles and C. G. Bauch, *Rev. Inorg. Chem.*, 1985, **7**, 315–339.

14 J. L. Falconer and A. E. Zagli, *J. Catal.*, 1980, **62**, 280–285.

15 G. Du, S. Lim, Y. Yang, C. Wang, L. Pfefferle and G. L. Haller, *J. Catal.*, 2007, **249**, 370–379.

16 F. Ocampo, B. Louis, L. Kiwi-Minsker and A. C. Roger, *Appl. Catal., A*, 2011, **392**, 36–44.

17 J. Liu, C. Li, F. Wang, S. He, H. Chen, Y. Zhao, M. Wei, D. G. Evans and X. Duan, *Catal. Sci. Technol.*, 2013, **3**, 2627–2633.

18 Q. Pan, J. Peng, S. Wang and S. Wang, *Catal. Sci. Technol.*, 2014, **4**, 502–509.

19 G. Meng and G. Lu, *Catal. Commun.*, 2014, **54**, 55–60.

20 G. D. Weatherbee and C. H. Bartholomew, *J. Catal.*, 1984, **87**, 352–362.

21 J. Lahtinen, T. Anraku and G. A. Somorjai, *Catal. Lett.*, 1994, **25**, 241–255.

22 S. Alayoglu, S. K. Beaumont, F. Zheng, V. V. Pushkarev, H. Zheng, V. Iablokov, Z. Liu, J. Guo, N. Kruse and G. A. Somorjai, *Top. Catal.*, 2011, **54**, 778–785.

23 G. Zhou, T. Wu, H. Xie and X. Zheng, *Int. J. Hydrogen Energy*, 2013, **38**, 10012–10018.

24 D. J. Dwyer and G. A. Somorjai, *J. Catal.*, 1978, **52**, 291–301.

25 A. E. Aksoylu, Z. Misirli and Z. I. Onsan, *Appl. Catal., A*, 1998, **168**, 385–397.

26 J. Sehested, K. E. Larsen, A. L. Kustov, A. M. Frey, T. Johannessen, T. Bligaard, M. P. Andersson, J. K. Norskov and C. H. Christensen, *Top. Catal.*, 2007, **45**, 9–13.

27 A. C. Gluhoi, N. Bogdanchikova and B. E. Nieuwenhuys, *J. Catal.*, 2005, **232**, 96–101.

28 D. Yang, J. Li, M. Wen and C. Song, *Catal. Today*, 2008, **139**, 2–7.

29 L. Xu, H. Song and L. Chou, *ACS Catal.*, 2012, **2**, 1331–1342.

30 J. Park and E. W. McFarland, *J. Catal.*, 2009, **266**, 92–97.

31 H. Y. Kim, H. M. Lee and J. Park, *J. Phys. Chem. C*, 2010, **114**, 7128–7131.

32 L. Xu, H. Song and L. Chou, *Int. J. Hydrogen Energy*, 2013, **38**, 7307–7325.

33 G. Larsen and G. L. Haller, *Catal. Lett.*, 1989, **3**, 103–110.

34 P. Panagiotopoulou and D. I. Kondarides, *Appl. Catal., B*, 2011, **101**, 738–746.

35 F. Wang and G. Lu, *J. Phys. Chem. C*, 2009, **113**, 17070–17075.

36 K. Hadjiivanov, M. Mihaylov, D. Klissurski, P. Stefanov, N. Abadjieva, E. Vassileva and L. Mintchev, *J. Catal.*, 1999, **185**, 314–323.

37 S. Tomiyama, R. Takahashi, S. Sato, T. Sodsawa and S. Yoshida, *Appl. Catal., A*, 2003, **241**, 349–361.

38 F. Pompeo, N. N. Nichio, M. G. Gonzalez and M. Montes, *Catal. Today*, 2005, **107**, 856–862.

39 Y. Pan, C. Liu and P. Shi, *J. Power Sources*, 2008, **176**, 46–53.

40 E. Lv, H. Zhang, Y. Yang and J. Ren, *J. Mol. Catal. (China)*, 2012, **26**, 333–339.

41 S. Shi, Y. Wang, J. Ma, L. Zheng, R. Yao and L. Zhou, *J. Mol. Catal. (China)*, 2013, **27**, 539–547.

42 R. B. Shalvoy, P. J. Reucroft and B. H. Davis, *J. Catal.*, 1979, **56**, 336–348.

43 F. Ocampo, B. Louis and A. C. Roger, *Appl. Catal., A*, 2009, **369**, 90–96.

44 Z. Li, X. Hu, L. Zhang, S. Liu and G. Lu, *Appl. Catal., A*, 2012, **417**, 281–289.

45 K. J. Williams, A. B. Boffa, J. Lahtinen, M. Salmeron, A. T. Bell and G. A. Somorjai, *Catal. Lett.*, 1990, **5**, 385–394.

46 M. P. Andersson, F. Abild-Pedersen, I. N. Remediakis, T. Bligaard, G. Jones, J. Engbæk, O. Lytken, S. Horch, J. H. Nielsen, J. Sehested, J. R. Rostrup-Nielsen, J. K. Norskov and I. Chorkendorff, *J. Catal.*, 2008, **255**, 6–19.

47 H. Olcay, Y. Xu and G. W. Huber, *Green Chem.*, 2014, **16**, 911–924.

48 M. Kilo, M. Hund, G. Sauer, A. Baiker and A. Wokaun, *J. Alloys Compd.*, 1996, **236**, 137–150.

49 Z. Zhang, J. Feng, Z. Wang, F. Yang, Q. Guo and J. Guo, *J. Chem. Phys.*, 2011, **236**, 144702.

50 A. Biswas, P. B. Rossen, C. Yang, W. Siemons, M. Jung, I. K. Yang, R. Ramesh and Y. H. Jeong, *Appl. Phys. Lett.*, 2011, **98**, 051904.

51 F. Sanchez, C. Ocal and J. Fontcuberta, *Chem. Soc. Rev.*, 2014, **43**, 2272–2285.

52 D. Vlachos, M. Kamaratos, S. D. Foulias, C. Argirusis and G. Borchardt, *Surf. Sci.*, 2004, **550**, 213–222.

53 M. Tanaka, *Appl. Surf. Sci.*, 2014, **98**, 324–329.